Chinese Journal of Aeronautics, (2014),27(6): 1384–1389

Chinese Society of Aeronautics and Astronautics
& Beihang University

Chinese Journal of Aeronautics

cja@buaa.edu.cn
www.sciencedirect.com

High-order implicit discontinuous Galerkin schemes for unsteady compressible Navier–Stokes equations

Jiang Zhenhua, Yan Chao *, Yu Jian

School of Aeronautic Science and Engineering, Beihang University, Beijing 100191, China

Received 25 October 2013; revised 18 May 2014; accepted 9 September 2014
Available online 18 October 2014

KEYWORDS

Discontinuous Galerkin scheme;
GMRES solver;
High order;
Implicit Runge–Kutta method;
Unsteady flows

Abstract Efficient solution techniques for high-order temporal and spatial discontinuous Galerkin (DG) discretizations of the unsteady Navier–Stokes equations are developed. A fourth-order implicit Runge–Kutta (IRK) scheme is applied for the time integration and a multigrid preconditioned GMRES solver is extended to solve the nonlinear system arising from each IRK stage. Several modifications to the implicit solver have been considered to achieve the efficiency enhancement and meantime to reduce the memory requirement. A variety of time-accurate viscous flow simulations are performed to assess the resulting high-order implicit DG methods. The designed order of accuracy for temporal discretization scheme is validate and the present implicit solver shows the superior performance by allowing quite large time step to be used in solving time-implicit systems. Numerical results are in good agreement with the published data and demonstrate the potential advantages of the high-order scheme in gaining both the high accuracy and the high efficiency.

1. Introduction

In the past decade, interest in the use of discontinuous Galerkin (DG)[1,2] methods for compressible flow simulation has become more widespread in aerodynamics applications. The DG methods possess many attractive features, such as the capability to handle complicated geometries, the flexibility for h/p adaptation, the compact stencils, the nice mathematical properties of conservation, stability, and convergence.

However, in the DG methods, numerical algorithms of computing the unsteady flows have lagged behind.[3] Most time-dependent calculations have been carried out in conjunction with the explicit time-integration methods which suffer from a very restrictive time step especially for the high-order schemes and hence become notoriously inefficient when dealing with the low-reduced frequency phenomena. Therefore it is desirable to develop a fully implicit method for the unsteady flow computations in the context of the DG discretization.

Recently, many efforts have been made on the use of higher-order implicit temporal schemes[4–11] in order to more efficiently resolve the unsteady flow problems. The implicit Runge–Kutta (IRK) methods which are with nice mathematical characteristics, self-starting and easily implemented in a

* Corresponding author. Tel.: +86 10 82317019.
E-mail addresses: zhenhua122122@163.com (Z. Jiang), yanchao@buaa.edu.cn (C. Yan).

Peer review under responsibility of Editorial Committee of CJA.

ELSEVIER Production and hosting by Elsevier

http://dx.doi.org/10.1016/j.cja.2014.10.004

variable time-stepping mode[5] were extended for the DG schemes to solve the compressible Euler and Navier–Stokes equations in Refs. 8,9 respectively. In addition, the key to a competitive implicit scheme lies in the utilization of an efficient nonlinear solver, and for those methods described above, the multigrid solver[8,9] and Newton–Krylov solver[7,10] have been applied to solving the resulting implicit system at each time step. On the other hand, the authors of Ref. 12 examined the performance of various solution algorithms for the DG methods and concluded that the multigrid preconditioned GMRES solver yielded the most efficient and scalable algorithm. Inspired by this work, the present study has been able to extend their p-multigrid preconditioned GMRES solver[12] to time-dependent problems and develop efficient unsteady solution techniques for high-order temporal and spatial DG discretizations of the Navier–Stokes equations. We remark that the features of the designed implicit solution approaches include allowing quite large time step to be used in the unsteady calculation and achieving both the high efficiency and high accuracy without significant memory increase.

2. DG formulation

The unsteady Navier–Stokes equations are written as

$$\boldsymbol{s} = \nabla \boldsymbol{q} \tag{1}$$

$$\frac{\partial \boldsymbol{q}}{\partial t} + \nabla \cdot \boldsymbol{f}_{\mathrm{c}}(\boldsymbol{q}) - \nabla \cdot \boldsymbol{f}_{\mathrm{v}}(\boldsymbol{q}, \boldsymbol{s}) = \boldsymbol{0} \tag{2}$$

where $\boldsymbol{s}$ is the auxiliary variable, $\boldsymbol{q}$ the conservative state vector, $\boldsymbol{f}_{\mathrm{c}}(\boldsymbol{q})$ the inviscid flux tensor and $\boldsymbol{f}_{\mathrm{v}}(\boldsymbol{q}, \boldsymbol{s})$ the viscous flux tensor. In order to formulate the DG method, we introduce approximate solution $\boldsymbol{q}_{\mathrm{h}}$, $\boldsymbol{s}_{\mathrm{h}}$ and polynomial test function v_{h} on the cell K, and then the weak formulation for Eqs. (1) and (2) can be given as

$$\int_K v_{\mathrm{h}} \boldsymbol{s}_{\mathrm{h}} \mathrm{d}\Omega = \int_K v_{\mathrm{h}} \nabla \boldsymbol{q}_{\mathrm{h}} \mathrm{d}\Omega + \int_{\partial K} \left(\hat{\boldsymbol{q}}_{\mathrm{h}} - \boldsymbol{q}_{\mathrm{h}}^{-}\right) v_{\mathrm{h}}^{-} \boldsymbol{n} \mathrm{d}\sigma \tag{3}$$

$$\begin{aligned} &\int_K v_{\mathrm{h}} \frac{\partial \boldsymbol{q}_{\mathrm{h}}}{\partial t} \mathrm{d}\Omega + \int_{\partial K} v_{\mathrm{h}} (\boldsymbol{f}_{\mathrm{c}} - \boldsymbol{f}_{\mathrm{v}}) \cdot \boldsymbol{n} \mathrm{d}\sigma \\ &- \int_K \nabla v_{\mathrm{h}} \cdot (\boldsymbol{f}_{\mathrm{c}}(\boldsymbol{q}_{\mathrm{h}}) - \boldsymbol{f}_{\mathrm{v}}(\boldsymbol{q}_{\mathrm{h}}, \boldsymbol{s}_{\mathrm{h}})) \mathrm{d}\Omega = 0 \end{aligned} \tag{4}$$

where Ω is domain, σ the boundary of Ω, $\hat{\boldsymbol{q}}_{\mathrm{h}}$ the numerical flux function, the superscript $-$ denotes the values inside the cell K and $\boldsymbol{n}$ is the outward unit normal vector to the boundary. In this article the test (basic) function is chosen based on the Taylor series expansion at the cell centroid[13] and the method in Ref. 14 which involves spline interpolation technique is adopted here to treat the curved boundaries. A local Lax–Friedrichs numerical flux[1] is used to replace the flux $\boldsymbol{f}_{\mathrm{c}} \cdot \boldsymbol{n}$ and the viscous flux $\boldsymbol{f}_{\mathrm{v}} \cdot \boldsymbol{n}$ is approximated by the BR2 scheme.[15] Then by assembling all the elemental contributions together, the ultimate semi-discrete system of Eq. (4) is obtained as

$$\boldsymbol{M} \frac{\mathrm{d}\boldsymbol{q}}{\mathrm{d}t} + \boldsymbol{R}(\boldsymbol{q}) = \boldsymbol{0} \tag{5}$$

where $\boldsymbol{M}$ denotes the mass matrix and $\boldsymbol{R}(\boldsymbol{q})$ the residual vector.

3. Temporal discretization

3.1. High-order IRK scheme

We choose a six-stage, fourth-order accurate IRK scheme, which is thus denoted as IRK4 in this work. The formula for the IRK4 scheme can be expressed as

$$\begin{cases} \boldsymbol{q}^{(0)} = \boldsymbol{q}^n \\ \boldsymbol{q}^{(s)} = \boldsymbol{q}^n - \Delta t \sum_{j=1}^{s} a_{sj} \boldsymbol{M}^{-1} \boldsymbol{R}\left(\boldsymbol{q}^{(j)}\right) \quad (s = 1, 2, \ldots, 6) \\ \boldsymbol{q}^{n+1} = \boldsymbol{q}^{(6)} \end{cases} \tag{6}$$

where a_{sj} represents the Butcher coefficient,[4] define the nonlinear unsteady residual $\boldsymbol{R}_{\mathrm{e}}$ and reformulate the IRK4 scheme as

$$\begin{aligned} \boldsymbol{R}_{\mathrm{e}}\left(\boldsymbol{q}^{(s)}\right) &= \frac{\boldsymbol{M}}{\Delta t} \boldsymbol{q}^{(s)} + a_{ss} \boldsymbol{R}\left(\boldsymbol{q}^{(s)}\right) \\ &- \left[\frac{\boldsymbol{M}}{\Delta t} \boldsymbol{q}^n - \sum_{j=1}^{s-1} a_{sj} \boldsymbol{R}\left(\boldsymbol{q}^{(j)}\right)\right] = \boldsymbol{0} \quad (s = 1, 2, \ldots, 6) \end{aligned} \tag{7}$$

Eq. (7) is solved with the basic idea proposed in Ref. 16 which introduces quasi-Newton subiteration time step to converge the resulted nonlinear system of each stage and therefore only uses the physical time step. Clearly, efficiently driving the unsteady residual to zero is crucial to the success of the IRK scheme.

3.2. Modified multigrid preconditioned GMRES solver

In order to solve the nonlinear system of Eq. (7), the GMRES solver originally developed in Ref. 12 for steady flows is extended here to solve this time-implicit system. The distinctive feature of the solver employs a proper cycling strategy for multigrid DG solution. Like Ref. 8, we restrict ourselves to the use of the p-multigrid alone. Furthermore, both the line-implicit and the point-implicit linearized Gauss–Seidel (LGS) relaxation methods are considered as smoothers of each multigrid level.

Since the Jacobian matrices are involved in the GMRES algorithm as well as in the LGS smoother, it is important to efficiently form the full Jacobian matrix. In the current work we apply the numerical procedure in Ref. 17, which was designed to evaluate the diagonal block matrix, here to compute those off-diagonal components of the Jacobian matrices as well.

Specifically for the cell K, we have the expression of off-diagonal matrices for the neighboring cells nb as

$$\frac{\partial \boldsymbol{R}_K}{\partial \boldsymbol{q}_{\mathrm{nb}}} \approx \frac{\boldsymbol{R}_K(\boldsymbol{q}_K, \boldsymbol{q}_{\mathrm{nb}} + \varepsilon) - \boldsymbol{R}_K(\boldsymbol{q}_K, \boldsymbol{q}_{\mathrm{nb}})}{\varepsilon} \tag{8}$$

where ε is a small parameter, e.g., $\varepsilon \approx \|\boldsymbol{q}_{\mathrm{nb}}\| \times 10^{-8}$. The method is computationally expensive. According to the recent and detailed research,[18] it requires $kN_{\mathrm{d}}N_{\mathrm{e}}$ times to evaluate the residual vector, where N_{d} is the number of degree, N_{e} is the number of equations and k depends on meshes. Therefore to improve the efficiency, a delayed matrix updating technique is further utilized, which only allows one evaluation for the Jacobian components during each entire time step.

In addition to the modification of evaluating and updating the Jacobian matrix, in the present solver the number of subcycles for solving the coarsest level problem remains 2.

And also different from the original method, we use a small number of GMRES iterations with fixed 1 restart and 3 Krylov basis throughout this paper. The benefit of such modifications is to reduce the memory increments due to the additional storage for the subspace basis, especially for the higher-order DG schemes. Moreover, there is no need for any kind of escaping strategies in this GMRES algorithm since a small number of iterations are adopted. The only stopping criterion for the designed approach is the termination of the nonlinear iterations and we choose the tolerance ratio 10^{-4} as Ref. 19.

Remark 1. While the employment of the high-order temporal discretization scheme IRK4 is an important part of the efficiency improvement, the adoption and modification of the GMRES solver described above are equally important aspects for the robustness and efficiency enhancement. We note that these are two key points that enable our method to use much larger time step sizes, thereby providing a competitive scheme for the unsteady flow simulations.
Remark 2. The simple choice of evaluating Jacobian matrix numerically and specifying parameters for the GMRES algorithm can lead us to treat the resulting implicit solver as a black box. Therefore for the practical DG code, it is easy to be implemented and extended to other implicit time-integration methods, such as widely used 2nd-order backwards differencing (BDF2) scheme.

4. Presentation of results

4.1. von-Karman vortex street

For the first case, we concentrate on assessing the accuracy and efficiency of the designed high-order IRK scheme. The von-Karman vortex street is chosen at Mach number $Ma_\infty = 0.1$, Reynolds number $Re_\infty = 150$ and has been performed on a 99×54 mesh with grid points clustered in the wake. The reference solutions are obtained with explicit three-stage Runge–Kutta method and the lift on the body is used as the representative measure of error.

Table 1 provides a detailed temporal refinement study with the IRK4 scheme. For the DG methods of various orders, the desired fourth order of accuracy of the IRK scheme is achieved within the range of time steps of interest. Fig. 1 depicts the required CPU time to obtain a preset level of error for the IRK4 and BDF2 schemes with different iteration termination tolerance. As the similar conclusions drawn in Ref. 8 for the Euler equations, here we demonstrate more performance

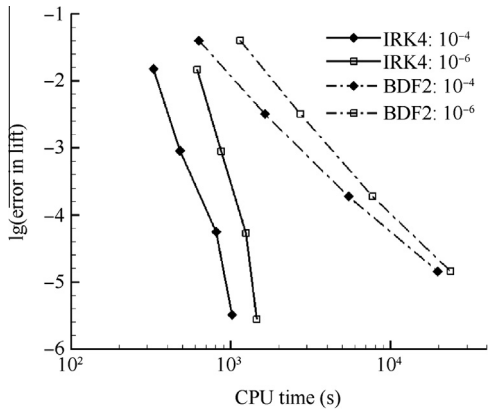

Fig. 1 Comparison of temporal efficiency between the BDF2 and IRK4 schemes with different termination tolerance.

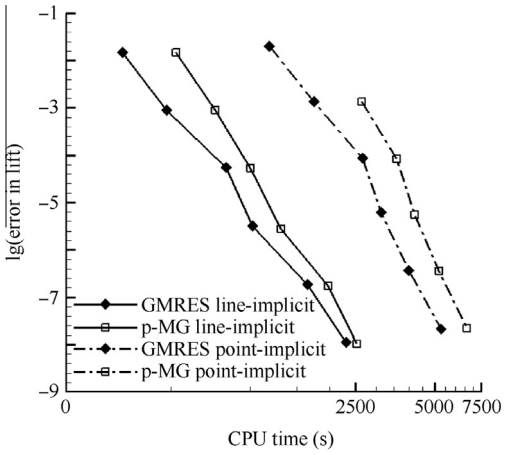

Fig. 2 Comparison of effectiveness between GMRES and p-multigrid method with different implicit smoothers.

improvement for the high-order temporal schemes for solving the Navier–Stokes equations. One can see for the accuracy level of 10^{-4} that the IRK4 scheme achieves almost one order of magnitude of speed-up relative to the BDF2 scheme. Also notable from the Fig. 1 is that decreasing the tolerance ratio has almost moved the curves uniformly, meaning the tolerance ratio 10^{-4} is small enough to ensure the convergence of the nonlinear iteration.[4]

Furthermore, the effectiveness of the GMRES solver has been verified in Fig. 2, where the present solver outperforms the p-multigrid (p-MG) method in terms of CPU time for both

Table 1 Temporal accuracy of the IRK4 scheme for the 2nd (P1), 3rd (P2) and 4th (P3) DG.

Time step	DG (P1)		DG (P2)		DG (P3)	
	L_2 error	Order	L_2 error	Order	L_2 error	Order
6.4	8.85×10^{-4}		1.68×10^{-3}		1.75×10^{-3}	
3.2	5.39×10^{-5}	4.04	1.04×10^{-4}	4.01	1.01×10^{-4}	4.11
1.6	3.10×10^{-6}	4.12	6.19×10^{-6}	4.07	6.21×10^{-6}	4.02
0.8	1.87×10^{-7}	4.05	3.69×10^{-7}	4.07	3.97×10^{-7}	3.97
0.4	1.10×10^{-8}	4.09	2.23×10^{-8}	4.05	2.51×10^{-8}	3.98
0.2	6.40×10^{-10}	4.09	1.35×10^{-9}	4.05	1.62×10^{-9}	3.95

the line-implicit and the point-implicit smoothers, in particular at larger time step, when the p-multigrid method coupled with the point-implicit smoother has even failed to converge. And it should be noted that compared to the p-multigrid method, the modified GMRES solver requires only 10% more memory at most, owing to our parameter choices for the steady-state solver. Fig. 3 further demonstrates the advantage of using large time step by giving quantitative comparison of the lift coefficients C_L obtained by the Runge–Kutta and IRK4 schemes. One can observe that the IRK4 is able to deliver comparable accuracy with only 4–5 points to resolve one shedding cycle, for which the computation time saved is nearly up to 2 orders of magnitude over the explicit counterpart.

4.2. Flow past an NACA0012 airfoil

The flow past a stationary NACA0012 airfoil is carried out with two different initial conditions. Case 1[20]: $Ma_\infty = 0.5$, $Re_\infty = 5000$, and angle of attack $\alpha = 2°$; Case 2[21]: $Ma_\infty = 0.2$, $Re_\infty = 5000$, and $\alpha = 10°$. A relatively coarse mesh consisting of 4050 triangular cells and relatively large time step size 0.2 are used in Case 1 in order to illustrate the importance of high-order schemes. As shown in Fig. 4, the unsteady wake is obtained only when the higher-order of accuracy in both the temporal and spatial discretizations is available. For Case 2, a much finer mesh containing 6864 quadrilateral and 31803 triangular elements is utilized. And still, we use a large time step of 0.1 in the computation. The vorticity fields computed by the 4th order DG coupled with IRK4 scheme are given in Fig. 5. Current results are well consistent with the solutions obtained with sufficiently refined mesh and much more restrictive time step size, see Fig. 6(f) in Ref. 21. Table 2 lists the computational efforts for the BDF2 and the IRK4 schemes for a comparable accuracy. The efficiency of the IRK4 scheme is clearly illustrated due to the ability to adopt much larger time step than the low order method.

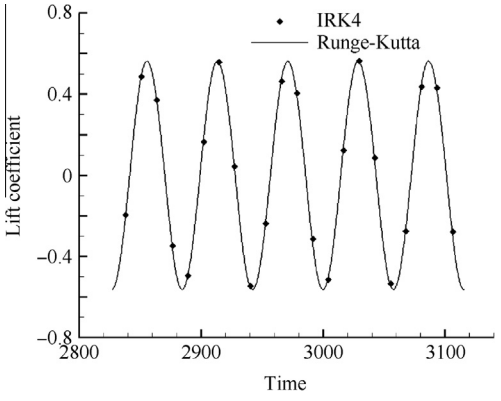

Fig. 3 Comparison of computed lift coefficients between the IRK4 and Runge–Kutta schemes for the 2nd order DG.

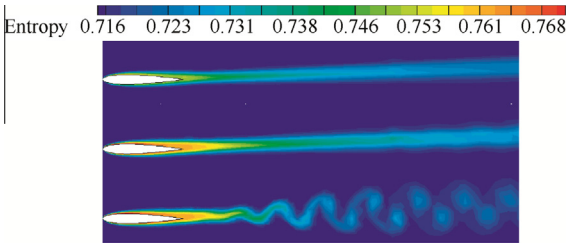

Fig. 4 Entropy contours obtained by DG (P1) with IRK4 (top), DG (P3) with BDF2 (middle) and DG (P3) with IRK4 (bottom) for Case 1.

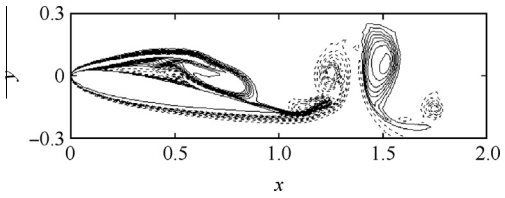

Fig. 5 Vorticity contour lines using 20 levels over the range ± 6 for Case 2.

Table 2 Comparison of computational efficiency between BDF2 and IRK4 schemes for Case 2.

Method	Time step size	CPU time (s)
BDF2	0.003	1.22×10^5
IRK4	0.100	1.81×10^4

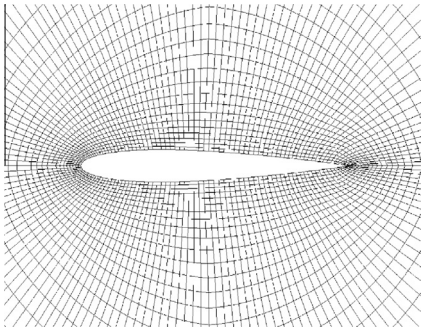

Fig. 6 O-type NACA0012 airfoil mesh.

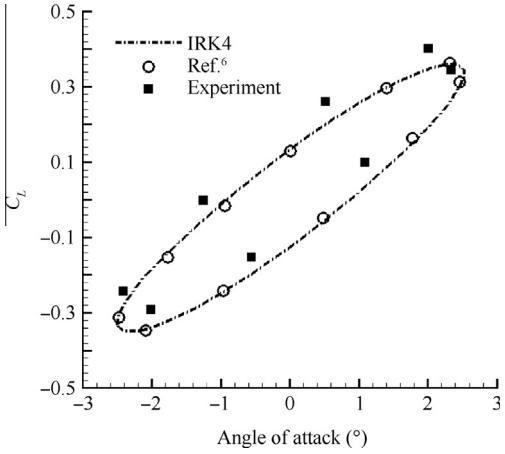

Fig. 7 Comparison of lift coefficients for flow past an O-type NACA0012 airfoil.

The flow over an oscillating NACA0012 airfoil has been used extensively in Refs. 6,11,22 for validation because of the availability of experimental data.[23] The airfoil undergoes harmonic pitching motion about the quarter chord with $\alpha = \alpha_m + \Delta\alpha\sin 2kt$, where $\alpha_m = 0.016°$, $\Delta\alpha = 2.51°$, and the reduced frequency $k = 0.0814$, and $Ma_\infty = 0.755$. In the current simulation, the Hermite weighted essentially non-oscillatory limiters are adopted and the computation is performed on an "O"-type mesh shown in Fig. 6. We compare the periodic lift coefficient versus the angle of attack in Fig. 7. One can see the present results agree well with the computational results in Ref. 6 although small discrepancy exists compared with the experimental data, which may be caused by the larger mean angle of attack in the experiment according to Ref. 22.

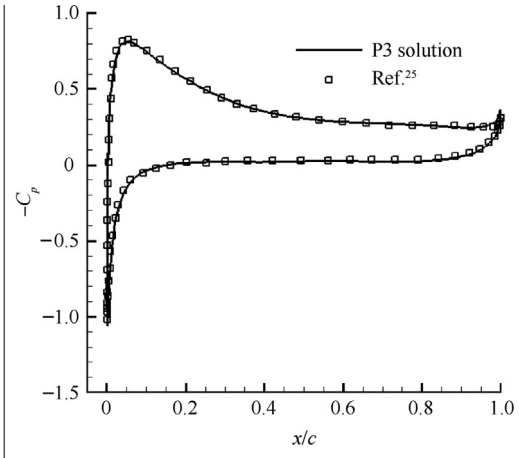

(a) Average pressure coefficient distribution

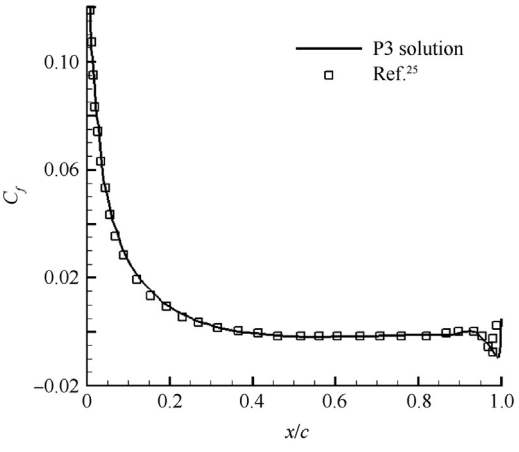

(b) Skin friction coefficient distribution

Fig. 8 Average pressure coefficient and skin friction coefficient distribution for flow past SD7003 airfoil.

Table 3 Measured and computed properties for flow past SD7003 airfoil.

Source	Separation (x/c)	Mean C_L	Mean C_D
Ref. 24	0.36	0.360	0.0470
Ref. 25	0.34	0.380	0.0504
Present result	0.36	0.375	0.0490

Table 4 Comparison of computational efficiency between BDF2 and IRK4 schemes for flow past SD7003 airfoil.

Method	Time step size	CPU time (s)
BDF2	0.0015	47300
IRK4	0.0400	8560

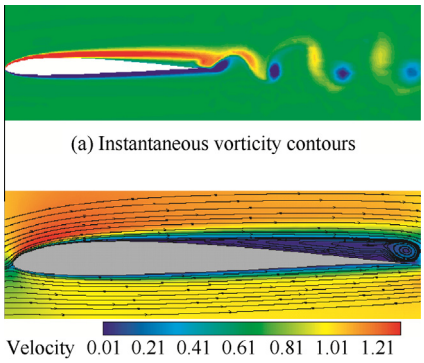

(a) Instantaneous vorticity contours

(b) Average velocity contours and streamlines

Fig. 9 Instantaneous vorticity contours and average velocity contours and streamlines for flow past SD7003 airfoil.

4.3. Flow past an SD7003 airfoil

For the last case we focus on the flow around the SD7003 airfoil with a laminar separation at $Ma_\infty = 0.2$, $Re_\infty = 1 \times 10^4$, and $\alpha = 4°$, which at this condition is fundamentally two-dimensional flow with available high-resolution numerical data.[24,25] The 4th-order DG and IRK4 scheme with fixed time step of 0.04 have been conducted on a hybrid mesh composed of 4428 quadrilateral cells and 12296 triangular cells. The surface pressure and skin friction coefficients C_f are shown in Fig. 8 and a summary of the computed properties of the flow is also listed in Table 3, where overall the results are seen to agree favorably with the previously published ones.

Fig. 9 presents the vorticity contours and velocity contours with streamlines for the flow features of separation on the upper surface and shedding of the tailing vortices. Notice how the combination of accurate time step and spatial discretization yields a solution with small dissipation that can capture the vortex propagation into the wake with high fidelity. Similarly, the temporal efficiency between the BDF2 and IRK4 scheme is compared in Table 4, where the IRK4 scheme requires about five times less CPU time for this case.

5. Conclusions

(1) Temporal convergence studies indicate that the current IRK4 scheme has achieved the designed order of accuracy. Additional modifications to the steady-state solver have been proved to be able to increase the computation efficiency of the unsteady algorithms with a small memory increment compared to the p-multigrid method.
(2) Numerical results of the von-Karman vortex street have demonstrated the efficiency gains by the use of high-order time integration scheme especially at tighter error

tolerances. The suggested GMRES solver has also shown the superior performance by enabling much larger time step to be used for both the line-implicit and the point-implicit smoothing strategies. And the advantages in accelerating the convergence of nonlinear systems are more noticeable for the larger time step.

(3) Numerical experiments for typical airfoil flows show the clear superiority of high-order schemes when implemented with the relatively coarse spatial and temporal resolution. Moreover, the present DG methods are able to capture all the relevant flow features of the unsteady separation and vortex shedding, and the computational results are in good agreement with the published data.

Further work will be carried out including the application of the present methods to more complex turbulent flow simulations.

References

1. Cockburn B, Shu CW. The Runge–Kutta discontinuous Galerkin method for conservation laws V: multidimensional systems. *J Comput Phys* 1998;**141**(1):199–224.
2. Cockburn B, Karniadakis G, Shu CW. The development of discontinuous Galerkin method. In: Cockburn B, Karniadakis G, Shu CW, editors. *Discontinuous Galerkin methods, theory, computation, and applications, lecture notes in computational science and engineering*. New York: Springer; 2000. p. 5–50.
3. Luo H, Segawa H, Visbal MR. An implicit discontinuous Galerkin method for the unsteady compressible Navier–Stokes equations. *Comput Fluids* 2012;**53**(1):133–44.
4. Bijl H, Carpenter MH, Vatsa VN, Kennedy CA. Implicit time integration schemes for the unsteady compressible Navier–Stokes equations: laminar flow. *J Comput Phys* 2002;**179**(1):313–29.
5. Jothiprasad G, Mavriplis DJ, Caughey DA. Higher order time integration schemes for the unsteady Navier–Stokes equations on unstructured meshes. *J Comput Phys* 2003;**191**(2):542–66.
6. Zhang LP, Wang ZJ. A block LU-SGS implicit dual time-stepping algorithm for hybrid dynamic meshes. *Comput Fluids* 2004;**33**(7):891–916.
7. Bijl H. Iterative methods for unsteady flow computations using implicit Runge–Kutta integration schemes. 2006. Report No.: AIAA-2006-1278.
8. Wang L, Mavriplis D. Implicit solution of the unsteady Euler equations for high-order accurate discontinuous Galerkin discretization. *J Comput Phys* 2007;**255**(2):1994–2015.
9. Segawa H, Luo H, Nourgaliev R. A diagonally implicit Runge–Kutta method for the discontinuous Galerkin solutions of the Navier–Stokes equations. 2011. Report No.: AIAA-2011-685.
10. Boom PD, Zingg DW. Time-accurate flow simulations using an efficient Newton–Krylov–Schur approach with high-order temporal and spatial discretization. 2013. Report No.: AIAA-2013-0383.
11. Yang XQ, Cheng SK, Yang AM, Sun G. Time spectral method for numerical simulation of unsteady viscous flow over oscillating airfoil and wing. *Acta Aeronaut Astronaut Sin* 2013;**34**(4):87–97 Chinese.
12. Shahbazi K, Mavriplis DJ, Burgess NK. Multigrid algorithms for high-order discontinuous Galerkin discretizations of the compressible Navier–Stokes equations. *J Comput Phys* 2009;**228**(21):7917–40.
13. Luo H, Baum JD, Löhner R. A discontinuous Galerkin method using Taylor basis for compressible flows on arbitrary grids. *J Comput Phys* 2008;**227**(20):8875–93.
14. Yu J, Yan C. Study on discontinuous Galerkin method for Navier–Stokes equations. *Chin J Theor Appl Mech* 2010;**42**(5):62–70 Chinese.
15. Bassi F, Crivellini A, Rebay S, Savini M. Discontinuous Galerkin solution of the Reynolds-averaged Navier–Stokes and k–ω turbulence model equations. *Comput Fluids* 2005;**34**(4):507–40.
16. Pulliam TH. Time accuracy and the use of implicit methods. 1993. Report No.: AIAA-1993-3360.
17. Sun Y, Wang ZJ, Liu Y. Efficient implicit non-linear LU-SGS approach for compressible flow computation using high-order spectral difference method. *Commun Comput Phys* 2009;**5**(2):760–78.
18. Xia Y, Luo H, Frisbey M, Nourgaliev R. A set of parallel, implicit methods for a reconstructed discontinuous Galerkin method for compressible flows on 3D hybrid grids. *Comput Fluids* 2014;**98**(7):134–51.
19. Zhang YF. Investigations of convergence acceleration and complex flow numerical simulation for high-order accurate scheme (WCNS) dissertation. Mianyang: China Aerodynamics Research and Development Center; 2007 [Chinese].
20. Kroll N. ADIGMA–A European project on the development of adaptive higher-order variational methods for aerospace applications. 2009. Report No.: AIAA-2009-176.
21. Hatakeyama N, Inoue O. Direct numerical simulation of noise from an airfoil in a uniform flow. 2006. Report No.: AIAA-2006-2504.
22. Batina JT. Unsteady Euler airfoil solutions using unstructured dynamic meshes. 1989. Report No.: AIAA-1989-0115.
23. Landon RH. NACA0012 oscillatory and transient pitching. 1982. Report No.: AGARD Report No. 702, Compendium of unsteady 379 aerodynamic measurements.
24. Galbraith M, Visbal M. Implicit large eddy simulation of low Reynolds number flow past the SD7003 airfoil. 2008. Report No.: AIAA-2008-225.
25. Uranga A, Persson P, Drela M, Peraire J. Implicit large eddy simulation of transitional flows over airfoils and wings. 2009. Report No.: AIAA-2009-4131.

Jiang Zhenhua received the B.S. degree in aeronautics science and engineering from Beihang University in 2009 and then became a Ph.D. candidate there. His main research interests are high-order numerical methods of the CFD.

Yan Chao received the Ph.D. from Tsinghua University in 1989 and worked as a postdoctoral researcher in Poitier university of France for several years. Now he is a professor of Beihang University. His current research interests include unsteady flows, LES, hybrid grid, optimization of aircraft.